

Characteristics of the electromagnetic wavepropagation inmagnetized plasma sheath and practical methodfor blackout mitigation

Xiang Wu(吴翔), Jiahui Zhang(张珈珲), Guoxiang Dong(董果香), and Lei Shi(石磊)

Citation: Chin. Phys. B, 2024, 33 (**5**): 055201. DOI: 10.1088/1674-1056/ad24d4
Journal homepage: http://cpb.iphy.ac.cn; http://iopscience.iop.org/cpb

What follows is a list of articles you may be interested in

Wave field structure and power coupling features of blue-core helicon plasma driven by various antenna geometries and frequencies

Chao Wang(王超), Jia Liu(刘佳), Lei Chang(苌磊), Ling-Feng Lu(卢凌峰), Shi-Jie Zhang(张世杰), and Fan-Tao Zhou(周帆涛)
Chin. Phys. B, 2024, 33 (**3**): 035201. DOI: 10.1088/1674-1056/ad1486

Effects of plasma radiation on the nonlinear evolution of neo-classical tearing modes in tokamak plasmas with reversed magnetic shear

Shuai Jiang(姜帅), Zheng-Xiong Wang(王正汹), Lai Wei(魏来), and Tong Liu(刘桐)
Chin. Phys. B, 2023, 32 (**10**): 105203. DOI: 10.1088/1674-1056/acedf7

Correction of intense laser-plasma interactions by QED vacuum polarization in collision of laser beams

Wen-Bo Chen(陈文博) and Zhi-Gang Bu(步志刚)
Chin. Phys. B, 2023, 32 (**2**): 025204. DOI: 10.1088/1674-1056/ac70b3

Parametric decay instabilities of lower hybrid waves on CFETR

Taotao Zhou(周涛涛), Nong Xiang(项农), Chunyun Gan(甘春芸), Guozhang Jia(贾国章), and Jiale Chen(陈佳乐)
Chin. Phys. B, 2022, 31 (**9**): 095201. DOI: 10.1088/1674-1056/ac67c2

Attenuation characteristics of obliquely incident electromagnetic wave in weakly ionized dusty plasma based on modified Bhatnagar-Gross-Krook collision model

Zhaoying Wang(王召迎), Lixin Guo(郭立新), and Jiangting Li(李江挺)
Chin. Phys. B, 2021, 30 (**4**): 045203. DOI: 10.1088/1674-1056/abe230

Characteristics of the electromagnetic wave propagation in magnetized plasma sheath and practical method for blackout mitigation

Xiang Wu(吴翔), Jiahui Zhang(张珈珲)†, Guoxiang Dong(董果香), and Lei Shi(石磊)

School of Aerospace Science and Technology, Xidian University, Xi'an 710071, *China*

(Received 30 October 2023; revised manuscript received 16 January 2024; accepted manuscript online 1 February 2024)

"Magnetic window" is considered as an effective method to solve the communication blackout issue. COMSOL software package based on the finite element method is utilized to simulate the propagation of right-handed circularly polarized wave in the magnetized plasma sheath. We assume a double Gaussian model of electron density and an exponential attenuation model of magnetic field. The propagation characteristics of right-handed circularly polarized wave are analyzed by the observation of the reflected, transmitted and loss coefficient. The numerical results show that the propagation of right-handed circularly polarized wave in the magnetized plasma sheath varies for different incident angles, collision frequencies, non-uniform magnetic fields and non-uniform plasma densities. We notice that reducing the wave frequency can meet the propagation conditions of whistle mode in the weak magnetized plasma sheath. And the transmittance of whistle mode is less affected by the variation of the electron density and the collision frequency. It can be used as a communication window.

Keywords: magnetized plasma sheath, communication blackout, finite element, incident angle, whistler wave

PACS: 52.35.Hr, 52.25.Xz, 52.25.Os **DOI:** 10.1088/1674-1056/ad24d4

1. Introduction

When a spacecraft re-enters the earth's atmosphere, it has to pass through near-Earth space in the altitude range of 20 km–100 km with a hypersonic velocity. During this process, the air at the head of the space vehicle is violently compressed, and a shock wave is created. The kinetic energy of the vehicle is partially converted into the internal energy of the air in the shock layer, leading to a dramatic increase in the air temperature and the consequent ionization and thermochemical reactions, which further generate plasma sheath encasing the space vehicle.[1] The plasma sheath contains a huge number of electrons, ions and dusts, which can significantly suppress electromagnetic (EM) wave transmission and greatly interfere with communication signals. This phenomenon is called "blackout".[2] To solve this problem, some strategies have been proposed, including strong static magnetic fields,[3] wave frequency modification,[4] $\boldsymbol{E}\times\boldsymbol{B}$ drift,[5] terahertz (THz) wave,[6–8] and so on. However, currently these methods are only theoretically feasible, and have technical limitations in practical application. Such as heat shielding configuration or heavy rain attenuation of THz wave.

In recent years, room-temperature superconducting materials have made significant advances in antimagnetism. It may make magnetization of the plasma sheath the most promising method to the blackout phenomenon. Magnetization of the plasma sheath first pointed out by Hodara in 1961,[9] which create a pass band (called "magnetic window") and allow the EM wave of a specific frequency to pass through the plasma sheath in the direction of the static magnetic field. Since then, many relevant studies have been carried out,[10–13] including simulation of sub-THz wave propagation in a magnetized non-uniform plasma sheath,[14] effects of nonuniform magnetic fields on the "magnetic window",[15] and study of electromagnetic wave propagation in an overdense magnetized collisional plasma sheath.[16] However, most of these studies focused on the effects of the non-uniform magnetic field, and studies on electron density, incident angle, and other relevant parameters are very limited. In this study, the propagation characteristics of right-handed circularly polarized wave in the plasma sheath with different incident angles, collision frequencies, non-uniform magnetic fields and non-uniform plasma densities are investigated. The frequency region of whistle mode minimally affected by different incident angles, collision frequencies, non-uniform magnetic fields and non-uniform plasma densities is determined. Based on the numerical results, a method for practical mitigation of blackout is proposed in this paper.

This paper is organized as follows. Equations and dispersion relations of circularly polarized wave in the magnetized plasma sheath taking into account the collision are given in Section 2. The emulational model used in this paper is presented in Section 3. Section 4 and Section 5 provide results and related discussion. Finally, conclusions are given in Section 6.

†Corresponding author. E-mail: zhangjh1@mail.ustc.edu.cn

© 2024 Chinese Physical Society and IOP Publishing Ltd

2. Wave equations and dispersion relations

In this paper, the electric field $\boldsymbol{E}$ of wave equation in the plasma sheath can be expressed as

$$\nabla\times(\nabla\times\boldsymbol{E})-k_0^2\left(\varepsilon-\frac{\boldsymbol{J}\sigma}{\omega\varepsilon_0}\right)\boldsymbol{E}=0, \tag{1}$$

$$\boldsymbol{E}(x,y,z)=\boldsymbol{E}(x,y)\mathrm{e}^{\mathrm{i}k_z z}, \tag{2}$$

where $k_0=\omega/c$, ω is circular frequency of high frequency wave fields, c is the speed of light in vacuum, ε_0 is the permittivity in vacuum, k_z is the component of the wave vector $\boldsymbol{k}$ in the z direction. $\boldsymbol{J}$ is the induced current in the plasma sheath, σ is the conductivity tensor, ε is the dielectric tensor. In Eq. (1), it involves the transformation of the dielectric tensor in the coordinate system of STIX frame[17] to the dielectric tensor in the coordinate system of this paper, where the non-uniform magnetic field $\boldsymbol{B}_0$ is aligned along y direction and the $\boldsymbol{k}$ is placed in xoy plane in the coordinate system of this paper. The transformation is given as

$$\varepsilon=\boldsymbol{G}^{-1}\cdot\varepsilon^{(\mathrm{STIX})}\cdot\boldsymbol{G}, \tag{3}$$

where $\boldsymbol{G}$ is the transformation matrix. It is given as

$$\boldsymbol{G}=\begin{bmatrix}1&0&0\\0&0&1\\0&-1&0\end{bmatrix}, \tag{4}$$

where $\varepsilon^{(\mathrm{STIX})}$ is the dielectric tensor in the coordinate system of STIX frame. It is given as

$$\varepsilon^{(\mathrm{STIX})}=\begin{bmatrix}\varepsilon_1&\varepsilon_2&0\\-\varepsilon_2&\varepsilon_1&0\\0&0&\varepsilon_3\end{bmatrix}, \tag{5}$$

where ε_1, ε_2, and ε_3 are the components of the $\varepsilon^{(\mathrm{STIX})}$. We assume that the ions are stationary at high wave frequency, thus in this paper the plasma density is replaced by the electron density. The components of the $\varepsilon^{(\mathrm{STIX})}$ in the magnetized plasma sheath taking into account the collision can be written as

$$\varepsilon_1=1+\frac{\mathrm{i}\omega_{\mathrm{pe}}^2(\nu_{\mathrm{e}}-\mathrm{i}\omega)}{\omega[(\nu_{\mathrm{e}}-\mathrm{i}\omega)^2+\omega_{\mathrm{ce}}^2]}, \tag{6}$$

$$\varepsilon_2=\frac{\mathrm{i}\omega_{\mathrm{pe}}^2\omega_{\mathrm{ce}}}{\omega[(\nu_{\mathrm{e}}-\mathrm{i}\omega)^2+\omega_{\mathrm{ce}}^2]}, \tag{7}$$

$$\varepsilon_3=1+\frac{\mathrm{i}\omega_{\mathrm{pe}}^2}{\omega(\nu_{\mathrm{e}}-\mathrm{i}\omega)}, \tag{8}$$

where ν_{e} is the collision frequency of electrons. ω_{pe} and ω_{ce} are electron plasma circular frequency and electron cyclotron circular frequency, respectively, which are given as

$$\omega_{\mathrm{pe}}=\sqrt{\frac{e^2n_{\mathrm{e}}}{m_{\mathrm{e}}\varepsilon_0}}, \tag{9}$$

$$\omega_{\mathrm{ce}}=\frac{eB_0}{m_{\mathrm{e}}}, \tag{10}$$

where e is the charge of the electron, n_{e} is the electron density. m_{e} is the mass of the electrons. B_0 is the scalar part of $\boldsymbol{B}_0$.

The EM wave propagating along the $\boldsymbol{B}_0$ direction in the magnetized plasma sheath can be mainly decomposed into left-handed circularly polarized wave (left-handed wave) and right-handed circularly polarized wave (right-handed wave). The dispersion relations of left-handed wave and right-handed wave in this paper are given as

$$\text{Right-handed wave}:\ n^2=\frac{c^2k^2}{\omega^2}=1-\frac{\omega_{\mathrm{pe}}^2/\omega^2}{1-(\omega_{\mathrm{ce}}/\omega)}, \tag{11}$$

$$\text{Left-handed wave}:\ n^2=\frac{c^2k^2}{\omega^2}=1-\frac{\omega_{\mathrm{pe}}^2/\omega^2}{1+(\omega_{\mathrm{ce}}/\omega)}, \tag{12}$$

where n is the refractive index. In Eqs. (11) and (12), we get the cut-off frequencies of left-handed wave and right-handed wave separately by setting $k=0$, which are given as

$$\omega_{\mathrm{R}}=\frac{1}{2}[\omega_{\mathrm{ce}}+(\omega_{\mathrm{ce}}^2+4\omega_{\mathrm{pe}}^2)^{1/2}], \tag{13}$$

$$\omega_{\mathrm{L}}=\frac{1}{2}[-\omega_{\mathrm{ce}}+(\omega_{\mathrm{ce}}^2+4\omega_{\mathrm{pe}}^2)^{1/2}], \tag{14}$$

the $1/n^2$ versus ω of left-handed wave and right-handed wave is shown in Fig. 1. We use the blue line to represent the left-handed wave and the green line to represent the right-handed wave. Wave can propagate in the magnetized plasma sheath while $1/n^2>0$. According to the findings depicted in Fig. 1, it is apparent that the propagation of the right-handed wave is viable within the magnetized plasma sheath when its frequency is lower than the electron cyclotron frequency. This specific frequency range is identified as being below the right-handed cut-off frequency, and is thoroughly examined in Subsection 4.1 for further elucidation. From Fig. 1 and Eq. (14) we can also find that the left-handed wave fails to propagate in the magnetized plasma sheath when the wave frequency is lower than the left-handed cut-off frequency, which means that its propagation is strictly limited by B_0 and n_{e}. While in the actual re-entry process, n_{e} is not completely controllable. Thus, the left-handed wave will not be concerned in this paper.

Notably, the above derivation between cut-off frequencies and dispersion relations is all based on the premise that the incident angle $\theta=0^\circ$ (θ is the angle between $\boldsymbol{k}$ and $\boldsymbol{B}_0$). For $\theta\neq0^\circ$, dispersion relations vary with $\boldsymbol{k}$. Therefore, we set up a control group in Section 4 with $\theta=0^\circ$ and $\theta=15^\circ$ separately to study the difference between oblique incidence ($\theta\neq0^\circ$) and direct incidence ($\theta=0^\circ$). And the effect due to different incident angles is further investigated in Subsection 4.4.

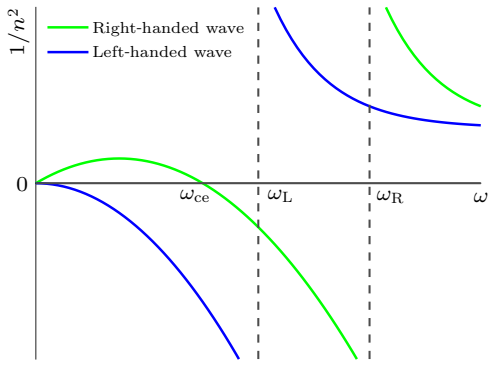


Fig. 1. The dispersion relations of right-handed wave and left-handed wave.

3. Simulation model

We employ the COMSOL Multiphysics software package, utilizing the finite element method (FEM), for addressing the interconnected wave equations within the frequency domain. We make the assumption that linear perturbation variables exhibited oscillations characterized by the time-harmonic term $e^{i\omega t}$. Figure 2 illustrates the two-dimensional (2D) simulation model of EM wave propagation in the magnetized plasma sheath, where $l_1 = l_3 = 0.1$ m and $l_2 = 0.3$ m.

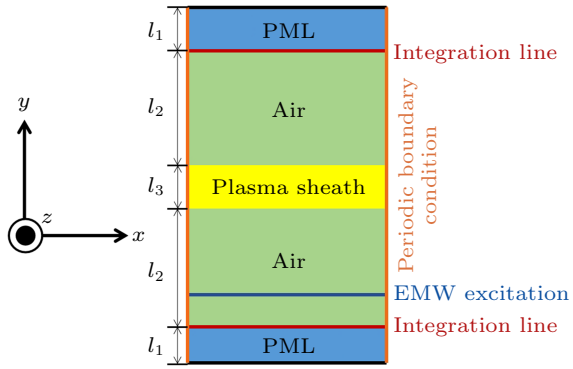


Fig. 2. Modeling of the EM wave across the non-uniformly magnetized plasma in the *xoy* plane of the Cartesian coordinate system.

3.1. Basic model setting

The initiation of EM wave excitation is positioned in the lower air region, with $\boldsymbol{k}$ of EM wave lying in the *xoy* plane. The mode of EM wave is right-handed circularly polarized wave. Electron density and magnetic field non-uniformities are assumed along y direction, while uniformity prevail in x and z directions. We apply periodic boundary conditions, for left and right boundary and employ perfect matched layers (PMLs) to model the air region extending infinitely. Wave frequencies span from 1 GHz to 40 GHz, with an input wave power of 1 W.

3.2. PML setting

In this paper, PML are used to simulate the infinite boundary conditions for EM waves. The electromagnetic property of the PML is the same as the air. The polynomial stretching function is applied in the y direction, which is given as

$$f_p(\xi) = s\xi p(1-\mathrm{i}), \tag{15}$$

where ξ is the dimensionless coordinate, which varies from 0 to 1 over the PML layer. s is a scaling factor. To retain perfect absorption for plane waves incident at an angle θ relative to the boundary normal, it is necessary to compensate for the longer wavelength seen by the PML in the stretching direction by setting the scaling factor

$$s = 1/\cos\theta, \tag{16}$$

where p is a curvature parameter, which is equal to the default value 1. The function returns a new, complex and stretched, coordinate interpreted as relative to the typical wavelength for each simulation frequency, which means that the complex displacement for stretching in a single direction is $\Delta = \lambda f_p(\xi) - L_{PML}\xi$. L_{PML} is the original thickness of the PML, and we set $L_{PML} = l_1 = 0.1$ m in this paper. λ is a typical wavelength.

3.3. Coefficient definition

We define two integration lines (red lines in Fig. 2) and one integration surface (yellow surface in Fig. 2) to calculate the transmitted coefficient, reflected coefficient and loss coefficient.

The integration line located at the upper air: the PML boundary calculates the transmitted coefficient C_T, which is used to evaluate the transmission efficiency of EM wave through the plasma sheath. The definition of C_T is

$$C_T = \frac{\int \mathrm{d}l\,(\boldsymbol{n}\cdot\boldsymbol{S})}{P_{in}}, \tag{17}$$

where $\boldsymbol{S}$ is the Poynting vector out of the plasma sheath, $\boldsymbol{n}$ is the unit vector normal to the integral line, and P_{in} is the input power of the EM wave source.

The integration line located at the bottom air: the PML boundary calculates the reflected coefficient C_R. The definition of C_R is

$$C_R = \left|\frac{\int \mathrm{d}l\,(\boldsymbol{n}\cdot\boldsymbol{S})}{P_{in}}\right|. \tag{18}$$

The integration surface calculates the loss coefficient C_L. The definition of C_L is

$$C_L = \frac{\omega\varepsilon_0}{2}\int \mathrm{d}S\left[\mathrm{Re}(\boldsymbol{E}^*\cdot\varepsilon^A\cdot\boldsymbol{E})\right], \tag{19}$$

where $\boldsymbol{E}^*$ is the conjugate part of $\boldsymbol{E}$, ε^A is the anti-hermitian part of $\varepsilon^{(STIX)}$.

3.4. Electron density setting

During the practical re-entry process, electron density within the plasma sheath follows a distribution pattern characterized by lower density near the interface, reaching its maximum at a specific distance from the vehicle. Experimental

findings on plasma sheath behavior[18] suggest that the electron density profile could be accurately represented by double Gaussian model. In addition, Ouyang *et al.*[19] showed the electron collision frequency distribution and electron density distribution in the plasma sheath at different re-entry altitudes. The value of n_e ranges from 4.9×10^{15} m^{-3} to 4.3×10^{21} m^{-3}, while the value of ν_e spans from 0.1 GHz to 100 GHz. Thus, we utilize the double Gaussian model to simulate electron density distribution and select four clusters of electron densities commonly observed in the plasma sheath at different re-entry heights as the maximum values of double Gaussian models, which are 5×10^{17} m^{-3}, 1×10^{18} m^{-3}, 5×10^{18} m^{-3}, and 1×10^{19} m^{-3}, respectively (shown in Fig. 8).

3.5. Electron collision frequency setting

Compared to the electron density distribution, the estimation error of the electron collision frequency distribution is significant. The estimation error is approximately within an order of magnitude, which implies that providing an exact profile of the collision frequency distribution is of limited significance. Besides, the impact of the electron collision frequency distribution on the wave field is negligible. Therefore, selecting a set of constants to determine the electron collision frequency is adequate. We similarly choose four common groups of electron collision frequencies at different re-entry heights as control experiments, which are 0.5 GHz, 5 GHz, 10 GHz, and 50 GHz, respectively.

3.6. Magnetic field setting

We assume that a rectangular magnet is used to excite the non-uniform magnetic field. Guo *et al.*[20] indicated that the magnetic induction in the x, z directions could be much smaller than that in the y direction by proper placement of the rectangular magnet, which means that the effects of magnetic induction in the x, z directions can be neglected in this paper. The magnetic field distribution of some typical rectangular magnets within the plasma sheath can be approximately modeled using the Biot–Savart's law.[21] Thus, we assume that the direction of $\boldsymbol{B}_0$ is along the y axis and that the magnitude of $\boldsymbol{B}_0$ follows an exponential attenuation (shown in Fig. 3).

3.7. Mesh setting and convergence

We select mapped mesh form for simulation across all mesh configurations. Zhang *et al.*[22] indicated that the calculation error can be controlled in $\pm1\%$ if the mesh size in the x direction is less than $0.1\lambda_x$ and the mesh size in the y direction is less than $0.1\lambda_y$, approximately. λ_x and λ_y are the wavelength in the x and y directions. Therefore, the plasma sheath's mesh size in x and y directions is respectively adjusted to 5 mm and 0.33 mm to make sure that the calculation error is controlled in $\pm1\%$. We adjust the mesh size to 2.5 mm and 0.17 mm, 1 mm, and 0.06 mm for x and y directions respectively for numerical simulations, and the results such as transmitted coefficients remain the same, which indicate that the mesh size has met the convergence requirement.

4. Numerical results and discussion

4.1. Dependence on non-uniform magnetic fields

The distribution of B_0 in the plasma sheath is illustrated in Fig. 3. The maximum values of B_0 are 0.25 T, 0.5 T, 0.9 T, and 1.5 T, respectively. The maximum value of n_e is 5×10^{18}/m^3 and ν_e is 0.5 GHz. Grantham has confirmed that the communication blackout occurs when the power attenuation is more than 40 dB.[23] Thus, we assume that the wave can penetrate the plasma sheath when the transmitted coefficient is greater than -40 dB.

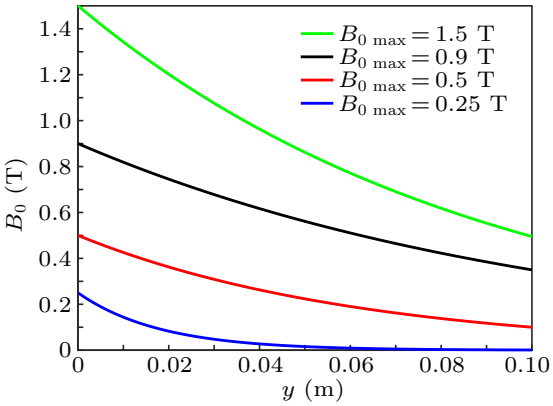


Fig. 3. The distribution of non-uniform magnetic field in the plasma sheath.

Reflected, transmitted and loss coefficients versus wave frequency for different non-uniform magnetic fields in the plasma sheath at $\theta=0°$ and $\theta=15°$ are shown in Figs. 4 and 5. We use the dashed lines to represent the minimum values of electron cyclotron frequency f_{ce} ($f_{ce}=\omega_{ce}/2\pi$) and the dotted lines to represent the maximum values of right-handed cut-off frequency f_R ($f_R=\omega_R/2\pi$). It can be seen from Fig. 4 that when the wave frequency is less than the minimum value of f_{ce}, the transmitted coefficient is greater than -40 dB. Wave in this frequency region is known as whistle mode, which can penetrate the plasma sheath to send information. Obviously, the minimum value of f_{ce} is a turning point. For the wave frequency exceeds the minimum value of f_{ce}, the transmitted coefficient drops dramatically to well below -40 dB. This frequency region is known as the cut-off region, wave in this cut-off region fail to penetrate the plasma sheath. As the wave frequency gradually increases to the maximum values of f_R, the transmission coefficient increases sharply to

above −40 dB. It indicates that the maximum values of f_R is another turning point. At this point, wave can penetrate the plasma sheath again. And wave in this frequency region is called the high frequency right-handed wave. From Eqs. (10) and (11), we know that f_{ce} and f_R increase with non-uniform magnetic field. As shown in the comparison of Figs. 4(a)–4(d), non-uniform magnetic field simultaneously affects the propagation of whistle mode and the high frequency right-handed wave in the plasma sheath.

When we excite right-handed wave, the electric vectors of the wave rotate clockwise with time along the direction of $\boldsymbol{k}$. For $\theta = 0°$, $\boldsymbol{k}$ is parallel to $\boldsymbol{B}_0$. The electric vectors of the wave are right-handed when we observe in the direction along $\boldsymbol{B}_0$. For $\theta = 15°$, $\boldsymbol{k}$ is no longer parallel to $\boldsymbol{B}_0$. At this point we observe in the direction along $\boldsymbol{B}_0$, the electric vectors of the wave have both left-handed and right-handed components. Since the cut-off frequency of left-handed wave is lower than that of right-handed wave, resulting in left-handed wave that can penetrate the plasma sheath in the cut-off region of right-handed wave. Thus, the transmission coefficient in cut-off region with $\theta = 15°$ increases to more than −40 dB for the strong magnetic field, as shown in Figs. 5(c)–5(d).

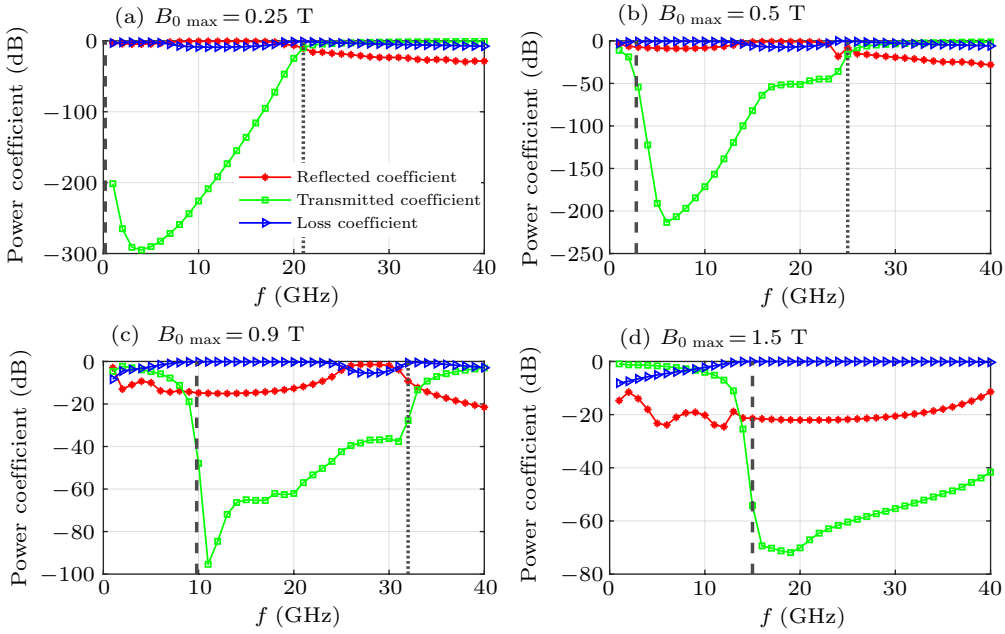


Fig. 4. Reflected, transmitted, and loss coefficients versus right-handed wave frequency for different non-uniform magnetic fields in the plasma sheath, $\nu_e = 0.5$ GHz, $\theta = 0°$, $n_{e\,max} = 5 \times 10^{18}$ m^{-3}. Dashed lines indicate the minimum values of f_{ce} and dotted lines indicate the maximum values of f_R. (a) $B_{0\,max} = 0.25$ T, (b) $B_{0\,max} = 0.5$ T, (c) $B_{0\,max} = 0.9$ T, (d) $B_{0\,max} = 1.5$ T.

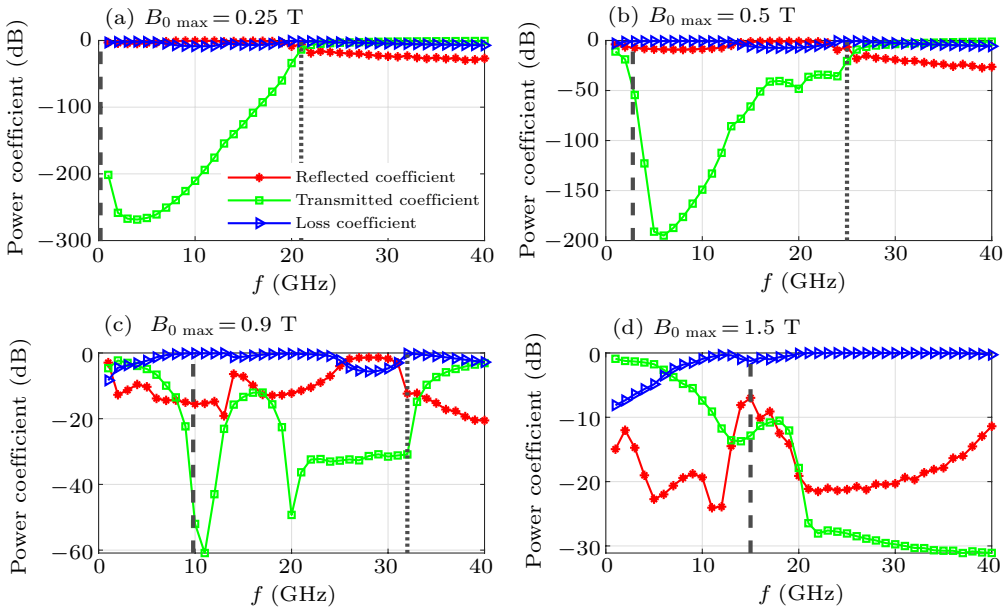


Fig. 5. Reflected, transmitted, and loss coefficients versus right-handed wave frequency for different non-uniform magnetic fields in the plasma sheath, $\nu_e = 0.5$ GHz, $\theta = 15°$, $n_{e\,max} = 5 \times 10^{18}$ m^{-3}. Dashed lines indicate the minimum values of f_{ce} and dotted lines indicate the maximum values of f_R. (a) $B_{0\,max} = 0.25$ T, (b) $B_{0\,max} = 0.5$ T, (c) $B_{0\,max} = 0.9$ T, (d) $B_{0\,max} = 1.5$ T.

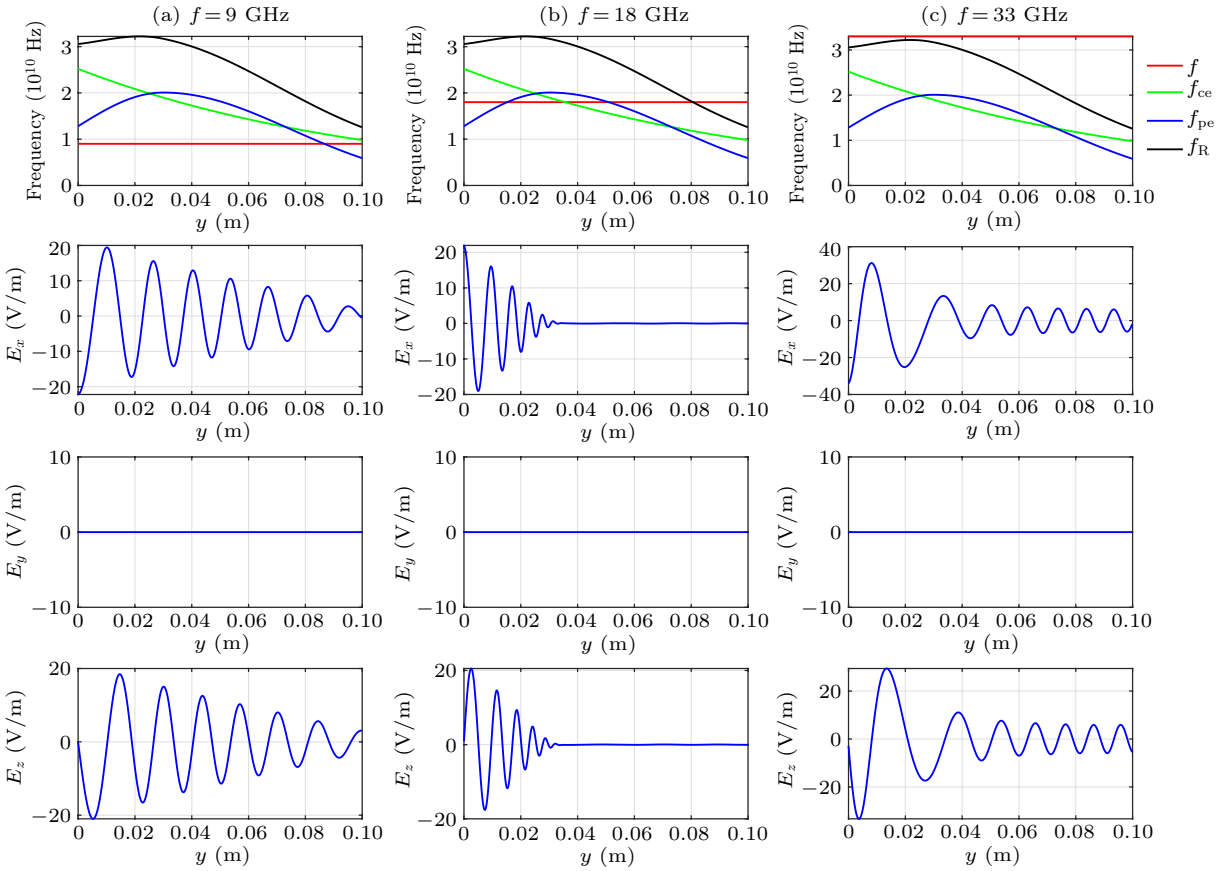


Fig. 6. The variation of the electric fields versus the plasma sheath for the different right-handed wave frequencies, $B_{0\,\max} = 0.9$ T, $n_{e\,\max} = 5 \times 10^{18}$ m^{-3}, $\nu_e = 0.5$ GHz, $\theta = 0°$. (a) $f = 9$ GHz, (b) $f = 18$ GHz, (c) $f = 33$ GHz.

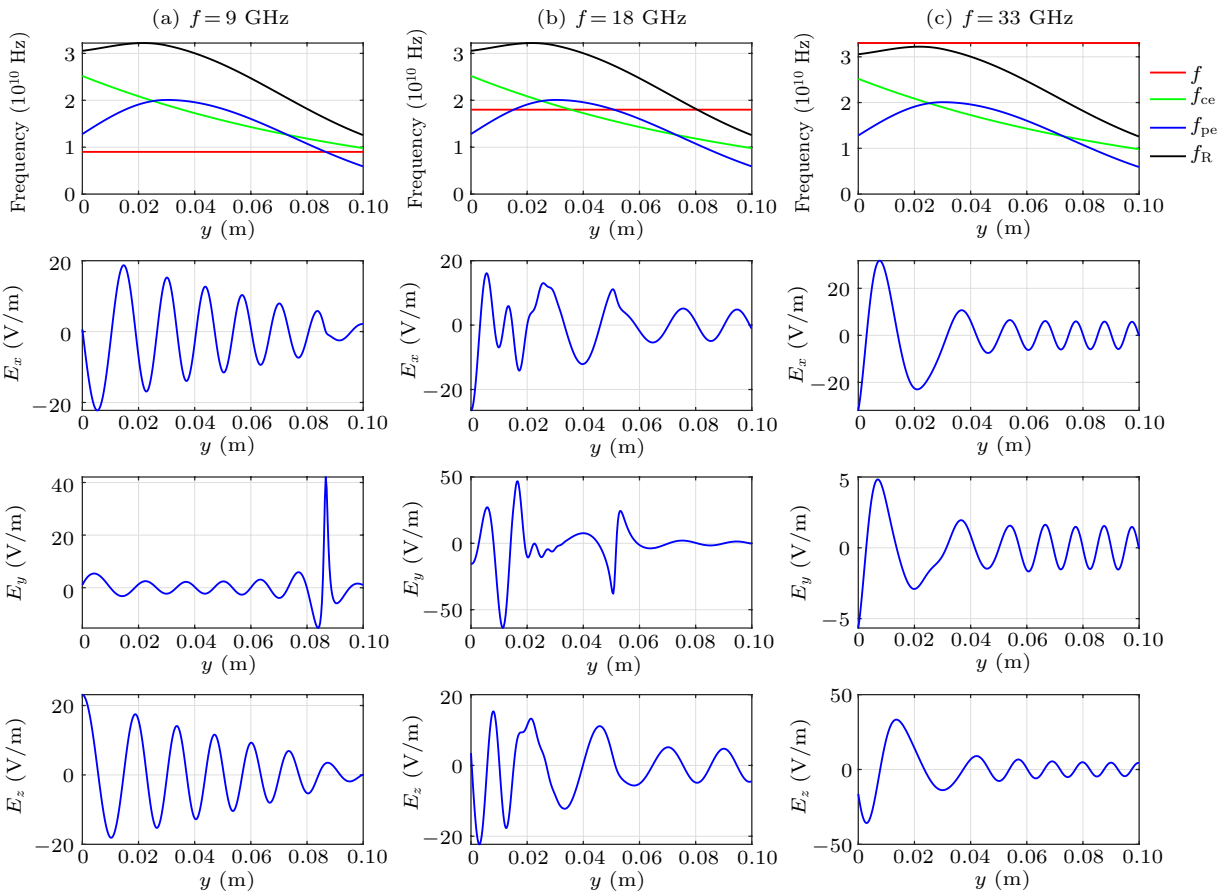


Fig. 7. The variation of the electric fields versus the plasma sheath for the different right-handed wave frequencies, $B_{0\,\max} = 0.9$ T, $n_{e\,\max} = 5 \times 10^{18}$ m^{-3}, $\nu_e = 0.5$ GHz, $\theta = 15°$. (a) $f = 9$ GHz, (b) $f = 18$ GHz, (c) $f = 33$ GHz.

The amplitude distributions of the electric field for different wave frequencies at $\theta = 0°$ and $\theta = 15°$ are shown in Figs. 6 and 7. Magnitude of the parameter is the same as panel (c) of Figs. 4 and 5. The minimum value of f_{ce} and the maximum value of f_R at this point are about 10 GHz and 32 GHz respectively. Wave frequencies are chosen to be 9 GHz, 18 GHz, and 33 GHz. The 9 GHz is less than the minimum value of f_{ce}, corresponding to the propagation of whistle mode. The 18 GHz is between the minimum value of f_{ce} and the maximum value of f_R, corresponding to wave propagation in the cut-off region. The 33 GHz is greater than the maximum value of f_R, corresponding to the propagation of the high frequency right-handed wave. For right-handed wave, k tends to infinity as wave frequency approaches f_{ce}, when wave resonates with the electronic oscillation. As shown in E_x and E_z of Fig. 6(b), the electron cyclotron resonance occurs at the position where f approaches f_{ce}. During the process of electron acceleration, the amplitude of the electric field severely attenuates. Wave loses energy and fails to penetrate the plasma sheath. Besides, the electron density is non-uniform along the y-axis direction. If wave can excite the electric field along the y-axis direction, which is parallel to the electron density gradient, it can generate the electron density perturbations to induce the plasma oscillation.[22] Thereafter, wave resonates with the plasma oscillation as f approaches f_{pe} ($f_{pe} = \omega_{pe}/2\pi$). From the comparison of E_y in Figs. 6 and 7, right-handed wave with $\theta = 15°$ excites the electric field along the y-axis direction. As shown in Figs. 7(a)–7(b), the plasma resonance occurs at the position where f approaches f_{pe}. The singularities appearance can be clearly observed at the plasma resonance occurrences.

4.2. Dependence on non-uniform electron densities

The distribution of n_e in the plasma sheath is illustrated in Fig. 8. The maximum values of n_e are 5×10^{17} m^{-3}, 1×10^{18} m^{-3}, 5×10^{18} m^{-3}, and 1×10^{19} m^{-3}, respectively. The maximum value of B_0 is chosen to 0.5 T and ν_e is chosen to 0.5 GHz.

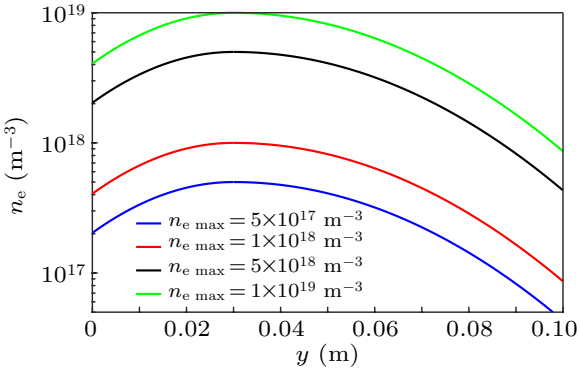


Fig. 8. The distribution of n_e in the plasma sheath.

Reflected, transmitted and loss coefficients versus wave frequency for the different electron densities in the plasma sheath at $\theta = 0°$ and $\theta = 15°$ are shown in Figs. 9 and 10. From Eqs. (9)–(11), we know that the value of f_R increases with the electron density, but the value of f_{ce} remains the same. As shown in the comparison of Figs. 9(a)–9(d), the electron density mainly affects the propagation of high frequency right-handed wave in the plasma sheath, while it has little effect on the propagation of low frequency whistle mode in the plasma sheath. Furthermore, it has been found that as f approaches f_{ce}, the transmitted coefficient decreases sharply with increasing electron density. This is attributed to the high participation of electrons in the electron cyclotron resonance.

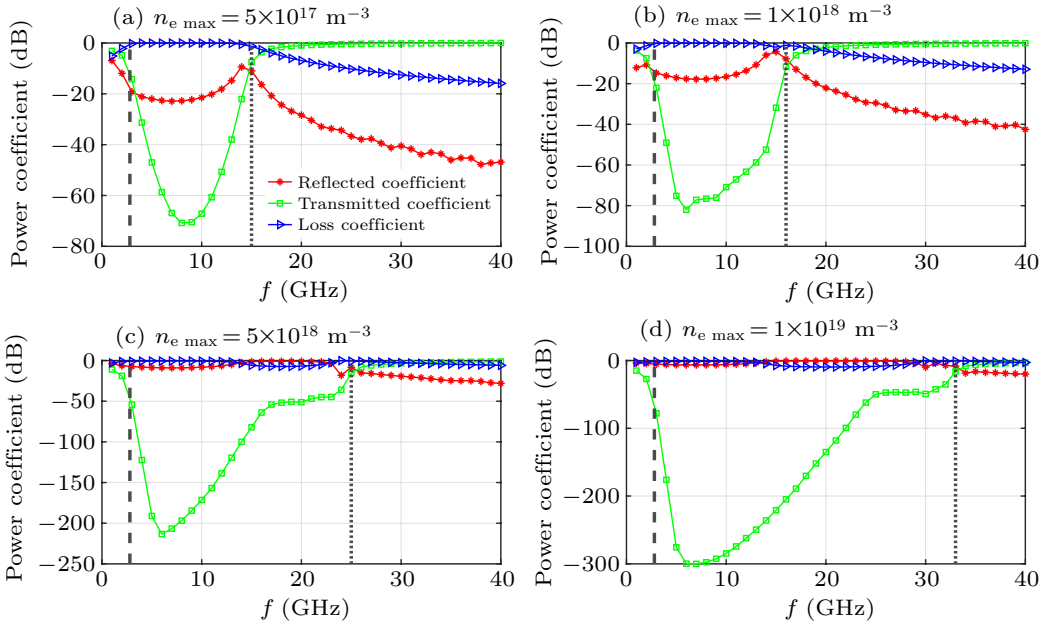


Fig. 9. Reflected, transmitted, and loss coefficients versus right-handed wave frequency for different electron densities in the plasma sheath, $\nu_e = 0.5$ GHz, $\theta = 0°$, $B_{0\,max} = 0.5$ T. Dashed lines indicate the minimum values of f_{ce} and dotted lines indicate the maximum values of f_R. (a) $n_{e\,max} = 5\times10^{17}$ m^{-3}, (b) $n_{e\,max} = 1\times10^{18}$ m^{-3}, (c) $n_{e\,max} = 5\times10^{18}$ m^{-3}, (d) $n_{e\,max} = 1\times10^{19}$ m^{-3}.

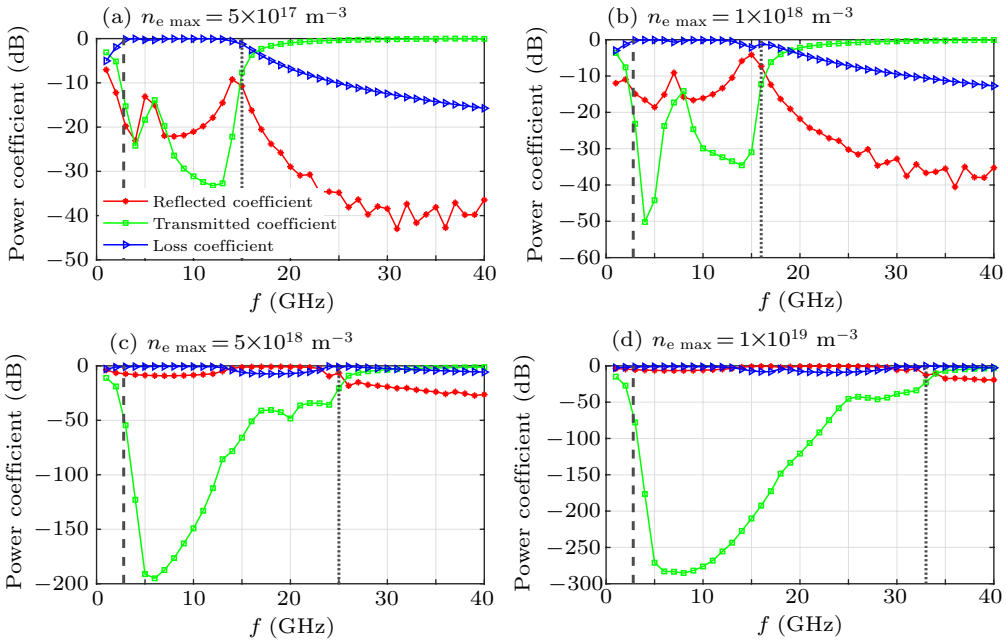


Fig. 10. Reflected, transmitted, and loss coefficients versus right-handed wave frequency for different electron densities in the plasma sheath, $\nu_e = 0.5$ GHz, $\theta = 15°$, $B_{0\,max} = 0.5$ T. Dashed lines indicate the minimum values of f_{ce} and dotted lines indicate the maximum values of f_R. (a) $n_{e\,max} = 5\times10^{17}$ m^{-3}, (b) $n_{e\,max} = 1\times10^{18}$ m^{-3}, (c) $n_{e\,max} = 5\times10^{18}$ m^{-3}, (d) $n_{e\,max} = 1\times10^{19}$ m^{-3}.

4.3. Dependence on the collision frequencies

The collision frequency ν_e is set to 0.5 GHz, 5 GHz, 10 GHz and 50 GHz, respectively. The maximum value of B_0 is chosen to 0.5 T and the maximum value of n_e is chosen to 5×10^{18} m^{-3}.

Reflected, transmitted, and loss coefficients versus right-handed wave frequency for different collision frequencies in the plasma sheath at $\theta = 0°$ and $\theta = 15°$ are shown in Figs. 11 and 12. We notice that the collision of free electrons with neutral particles dominates the process when f is less than f_{ce}, the transmitted coefficient decreases with increasing ν_e. Notably, there is a discernible shift in dominant mechanisms as f approaches and reaches f_{ce}, with electron cyclotron resonance taking precedence, transmitted coefficient increases with ν_e. As f beyond f_R, the dynamics revert to electron–neutral particle collisions being preeminent, thereby reviving the pattern of reducing transmitted coefficient with heightened ν_e. Moreover, from a comparison of Figs. 11(a)–11(d), the curve of the transmitted coefficient becomes flat as ν_e increases.

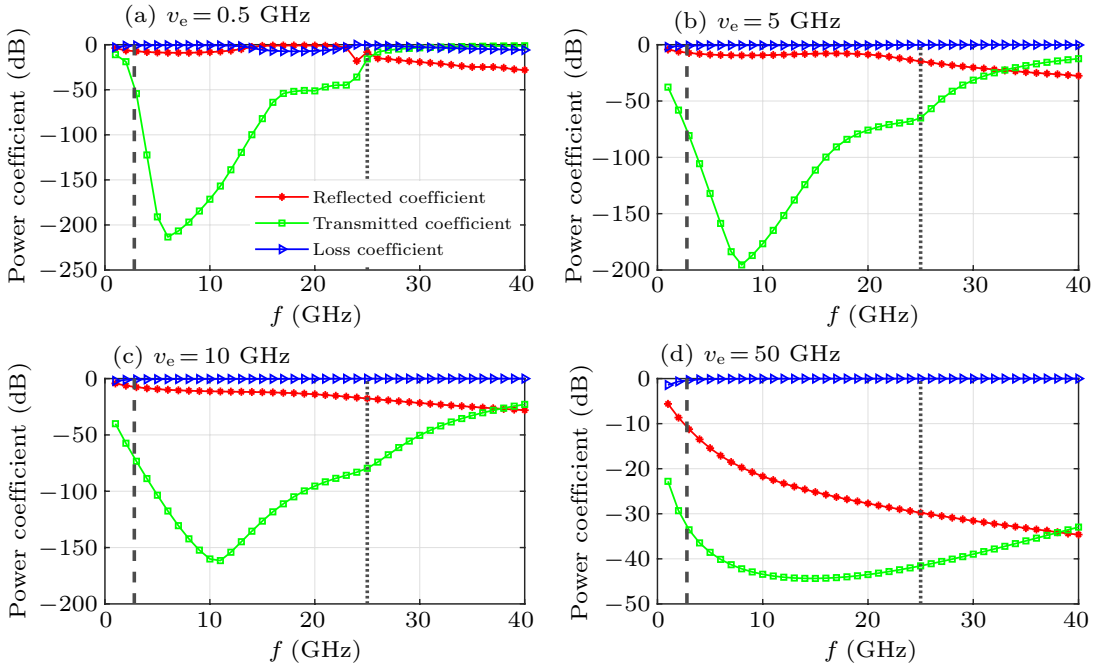


Fig. 11. Reflected, transmitted, and loss coefficients versus right-handed wave frequency for different collision frequencies in the plasma sheath, $B_{0\,max} = 0.5$ T, $\theta = 0°$, $n_{e\,max} = 5\times10^{18}$ m^{-3}. Dashed lines indicate the minimum values of f_{ce} and dotted lines indicate the maximum values of f_R. (a) $\nu_e = 0.5$ GHz, (b) $\nu_e = 5$ GHz, (c) $\nu_e = 10$ GHz, (d) $\nu_e = 50$ GHz.

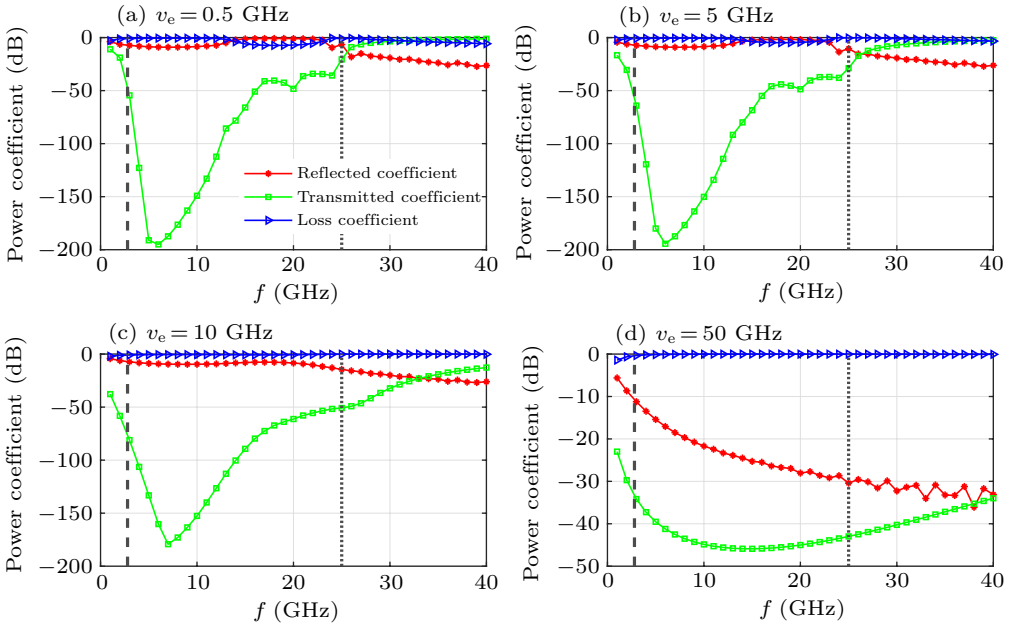


Fig. 12. Reflected, transmitted, and loss coefficients versus right-handed wave frequency for different collision frequencies in the plasma sheath, $B_{0\,\max} = 0.5$ T, $\theta = 15°$, $n_{e\,\max} = 5\times10^{18}$ m^{-3}. Dashed lines indicate the minimum values of f_{ce} and dotted lines indicate the maximum values of f_R. (a) $\nu_e = 0.5$ GHz, (b) $\nu_e = 5$ GHz, (c) $\nu_e = 10$ GHz, (d) $\nu_e = 50$ GHz.

4.4. Dependence on the incident angles

The incident angle θ is set to 0°, 15°, 30°, and 45°, respectively. The maximum value of B_0 is chosen to 0.5 T. The maximum value of n_e is chosen to 5×10^{18} m^{-3} and ν_e is chosen to 0.5 GHz.

Reflected, transmitted, and loss coefficients versus wave frequency for different incident angles in the plasma sheath is shown in Fig. 13. It is evident that the transmitted coefficient fluctuates with θ within the frequency range from 20 GHz to 30 GHz, which is primarily attributed to the alterations in plasma resonance and cut-off frequency. From Subsection 4.1 we know that only an oblique incident wave is capable of exciting the plasma resonance. As θ increases, the plasma resonance intensifies and the transmitted coefficient decreases. Besides, for $\theta \neq 0°$, k is given as

$$k^2 = k_x^2 + k_y^2, \tag{20}$$

where k_x and k_y are the components of the wave vector $\boldsymbol{k}$ in the x-axis and y-axis directions, respectively. With the wave frequency held constant, k remains the same and k_x increases with θ. Leading to an inverse relationship between k_y and increasing θ. The wave cuts off as k_y drops to zero. Thus, the cut-off frequency increases with θ.

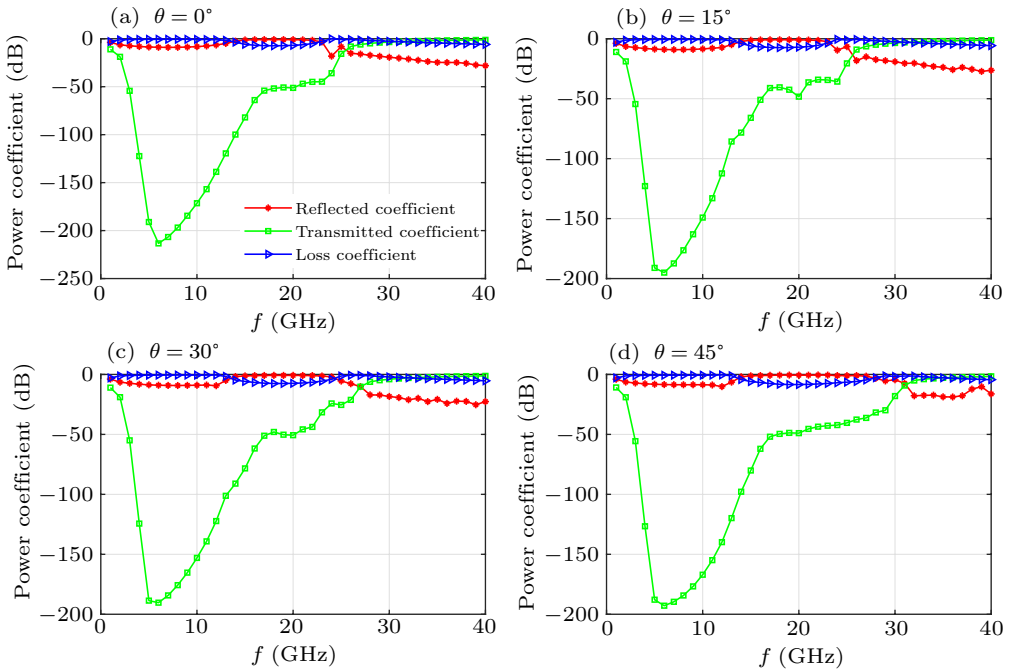


Fig. 13. Reflected, transmitted, and loss coefficients versus wave frequency for different incident angles in the plasma sheath, $\nu_e = 0.5$ GHz, $B_{0\,\max} = 0.5$ T, $n_{e\,\max} = 5\times10^{18}$ m^{-3}. (a) $\theta = 0°$, (b) $\theta = 15°$, (c) $\theta = 30°$, (d) $\theta = 45°$.

5. Practical method for blackout mitigation

In this section, simulation results are presented for the propagation of low-frequency whistle mode in various incident angles, collision frequencies, non-uniform magnetic fields, and plasma densities. Three sets of above parameters are fixed quantitatively, allowing for the isolated variation of a singular parameter to investigate its specific impact on the transmission coefficient of whistle mode. Wave frequency range for this simulation is demarcated between 0.1 GHz to 4 GHz, with intervals set at 0.1 GHz increments. The transmitted coefficient as a function of wave frequency for different parameters is shown in Fig. 14. The relevant parameters of Fig. 14 are listed in Table 1.

Within this spectrum, whistle mode has a high value of the transmitted coefficient for strong magnetized plasma sheath, as shown in Fig. 14(a). However, considering that strong non-uniform magnetic field has not been obtained practically at an acceptable weight and volume for space vehicles. In its present state $B_0 = 0.5$ T, whistle mode can penetrate the magnetized plasma sheath at a frequency of 0.1 GHz–1 GHz to transmit information effectively. Similarly, within this spectrum 0.1 GHz–1 GHz, the transmitted coefficients of whistle mode in Figs. 14(b)–14(d) are almost greater than −40 dB. Thus, whistle mode within wave frequency of 0.1 GHz to 1 GHz, subject to the limits of the non-uniform magnetic field, showcasing a heightened transmitted power when mediated by different parameters. It remains substantially unaffected by fluctuations in parameters such as ν_e, n_e, and θ, highlighting a considerable advantage over the left-handed wave which exhibits a dependency on the magnitude of electron density. In addition, whistle mode at this frequency region facilitates a more expansive propagation region as compared to the capabilities achieved with MHz wave.[24] Moreover, it precludes the necessity for high-frequency THz wave, thereby offering a more pragmatic and simplified approach to antenna design for space vehicles. In summary, low-frequency whistle mode presents a promising avenue for communication owing to its resilience to variations in the defined parameters.

Table 1. The parameters in the simulation.

Parameters \ Figures	(a)	(b)	(c)	(d)
$B_{0\,\max}$		0.5 T	0.5 T	0.5 T
ν_e	0.5 GHz		0.5 GHz	0.5 GHz
$n_{e\,\max}$	5×10^{18} m^{-3}	5×10^{18} m^{-3}		5×10^{18} m^{-3}
θ	0°	0°	0°	

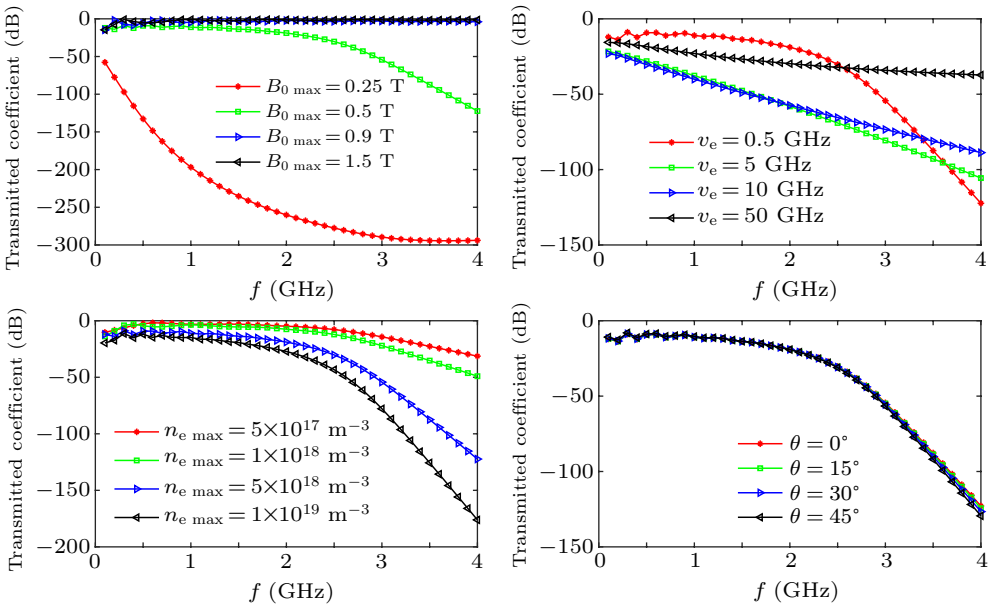


Fig. 14. Transmitted coefficient versus wave frequency for different parameters in the plasma sheath.

6. Conclusions

In order to use the "magnetic window" to solve the communication blackout issue. We employ finite element analysis software package COMSOL to model the propagation of right-handed circularly polarized wave in the magnetized plasma sheath, and investigate the effects of different incident angles, collision frequencies, non-uniform magnetic fields and non-uniform electron densities on the transmission response of right-handed circularly polarized wave. The results show that right-handed circularly polarized wave can penetrate the magnetized plasma sheath when the wave frequency is less than the minimum value of electron cyclotron frequency or greater than the maximum value of cut-off frequency of right-handed circularly polarized wave. The reason why right-handed wave cannot penetrate the magnetized plasma sheath is that electron cyclotron resonance drains the energy of right-handed wave as wave frequency approaches and reaches electron cy-

clotron frequency, while oblique incident wave (incident angle $\theta \neq 0$) also resonates with the plasma oscillations as wave frequency approaches and reaches electron plasma frequency. Cut-off frequency of right-handed circularly polarized wave mostly depends on the distribution of non-uniform magnetic field and non-uniform electron density, and electron cyclotron frequency mostly depends on the distribution of non-uniform magnetic field. Besides, incident angle and collision frequency affect right-handed wave propagation in the magnetized plasma sheath to a certain extent.

Based on the above findings, we investigate the transmitted power of low frequency whistle mode as affected by different incident angles, collision frequencies, non-uniform magnetic fields, and non-uniform plasma densities. Wave frequency range for this simulation is demarcated between 0.1 GHz to 4 GHz. The results show that subject to the limits of the non-uniform magnetic field, low-frequency whistle mode remains substantially unaffected by fluctuations in collision frequency, electron density, and incident angle within the frequency range of 0.1 GHz–1 GHz, which has a number of advantages compared to other waves. Such as simplifying the antenna design and expanding the propagation range of frequencies. The superior performance of whistle mode against perturbations due to variations in parameters enables it to be used as a communication window to send information.

Acknowledgements

Project supported by the National Natural Science Foundation of China (Grant Nos. 12275202, 62371372, 62101406, and 62001340), China Postdoctoral Science Foundation (Grant Nos. 2022M71490 and 2020M673341), the Innovation Capability Support Program of Shaanxi Province, China (Grant No. 2022TD-37), and the Natural Science Basic Research Program of Shaanxi Province, China (Grant No. 2023-JC-YB-549).

References

[1] Rybak J P and Churchill R J 1971 *IEEE Trans. Aerosp. Electron. Syst.* **AES-7** 879
[2] Liu Z W, Bao W M, Li X P, Liu D L and Bai B W 2015 *IEEE Trans. Plasma Sci.* **43** 3147
[3] Stenzel R L 1976 *Phys. Fluids* **19** 857
[4] Chen J M, Yuan K, Shen L F, Deng X H, Hong L J and Yao M 2016 *Prog. Electromagn. Res.* **157** 21
[5] Kim M, Keidar M and Boyd L D 2008 *J. Spacecr. Rockets* **45** 1223
[6] Wang M Y, Yu M X, Xu Z T, Li G P, Jiang B J and Xu J 2015 *IEEE Trans. Plasma Sci.* **43** 4182
[7] Wang M Y, Zhang M, Li G P, Jiang B J, Zhang X C and Xu J 2016 *Plasma Sci. Technol.* **18** 798
[8] Li J, Pi Y M and Yang X B 2014 *Wirel. Commun. Mob. Com.* **14** 1252
[9] Hodara H 1961 *Proc. IRE* **49** 1825
[10] Zhao Q, Xing X J, Xuan Y L and Liu S Z 2014 *Plasma Sci. Technol.* **16** 614
[11] Starkey R P 2015 *J. Spacecr. Rockets* **52** 426
[12] Liu J F, Ma H Y, Jiao Z H, Bai G H, Fang Y, Yi Y M and Xi X I 2020 *IEEE Trans. Plasma Sci.* **48** 2706
[13] Zhou H, Li X P, Xie K, Liu Y M, Yao B and Ai W 2017 *AIP Adv.* **7** 025114
[14] Yuan K, Shen L F, Yao M, Deng X H, Chen Z and Hong L J 2018 *Phys. Plasma* **25** 013302
[15] Zhou H, Li X P, Liu Y M, Bai B W and Xie K 2017 *IEEE Trans. Plasma Sci.* **45** 15
[16] Thoma C, Rose D V, Miller C L, Clark R E and Hughes T P 2009 *J. Appl. Phys.* **106** 043301
[17] Brambilla M 1999 *Plasma Phys. Controlled Fusion* **41** 1
[18] Rawhouser R 1971 *NASA Langley Res. Center* **252** 3
[19] Ouyang W C, Jin T, Wu Z W and Deng W F 2021 *IEEE Trans. Plasma Sci.* **49** 460
[20] Guo X F, Yang Y and Zheng X J 2004 *Appl. Math. Mech.* **25** 297
[21] Wang R K, Zuo H F and Meng L V 2011 *Aeronautical Comput. Techn.* **41** 19
[22] Zhang J H, Liu Y M, Li X P, Shi L, Yang M and Bai B W 2019 *AIP Adv.* **9** 055316
[23] Grantham W L 1971 *NASA Langley Res. Center* **252** 65
[24] Guo S S, Xie K, Sun B, Xi R Y and Liu Y 2021 *Plasma Science and Technology* **23** 075401